We are IntechOpen,
the world's leading publisher of
Open Access books
Built by scientists, for scientists

6,900
Open access books available

185,000
International authors and editors

200M
Downloads

154
Countries delivered to

Our authors are among the

TOP 1%
most cited scientists

12.2%
Contributors from top 500 universities

BOOK CITATION INDEX
CLARIVATE ANALYTICS
INDEXED

WEB OF SCIENCE™

Selection of our books indexed in the Book Citation Index
in Web of Science™ Core Collection (BKCI)

Interested in publishing with us?
Contact book.department@intechopen.com

Numbers displayed above are based on latest data collected.
For more information visit www.intechopen.com

Chapter

Convective Heat Transfer of Ethanol/Polyalphaolefin Nanoemulsion in Mini- and Microchannel Heat Exchangers for High Heat Flux Electronics Cooling

Jaime Rios, Mehdi Kabirnajafi, Takele Gameda, Raid Mohammed and Jiajun Xu

Abstract

The present study experimentally and numerically investigates the flow and heat transfer characteristics of a novel nanostructured heat transfer fluid, namely, ethanol/polyalphaolefin nanoemulsion, inside a conventionally manufactured minichannel of circular cross section and a microchannel heat exchanger of rectangular cross section manufactured additively using the Direct Metal Laser Sintering (DMLS) process. The experiments were conducted for single-phase flow of pure polyalphaolefin (PAO) and ethanol/PAO nanoemulsion fluids with two ethanol concentrations of 4 wt% and 8 wt% as well as for two-phase flow boiling of nanoemulsion fluids to study the effect of ethanol nanodroplets on the convective flow and heat transfer characteristics. Furthermore, the effects of flow regime of the working fluids on the heat transfer performance for both the minichannel and microchannel heat exchangers were examined within the laminar and transitional flow regimes. It was found that the ethanol/PAO nanoemulsion fluids can improve convective heat transfer compared to that of the pure PAO base fluid under both single- and two-phase flow regimes. While the concentration of nanoemulsion fluids did not reflect a remarkable distinction in single-phase heat transfer performance within the laminar regime, a significant heat transfer enhancement was observed using the nanoemulsion fluids upon entering the transitional flow regime. The heat transfer enhancement at higher concentrations of nanoemulsion within the transitional regime is mainly attributed to the enhanced interaction and interfacial thermal transport between ethanol nanodroplets and PAO base fluid. For two-phase flow boiling, heat transfer coefficients of ethanol/PAO nanoemulsion fluids were further enhanced when the ethanol nanodroplets underwent phase change. A comparative study on the flow and heat transfer characteristics was also implemented between the traditionally fabricated minichannel and additively manufactured microchannel of similar dimensions using the same working fluid of pure PAO and the same operating conditions. The results revealed that although the DMLS fabricated microchannel posed a higher pressure loss, a substantial heat
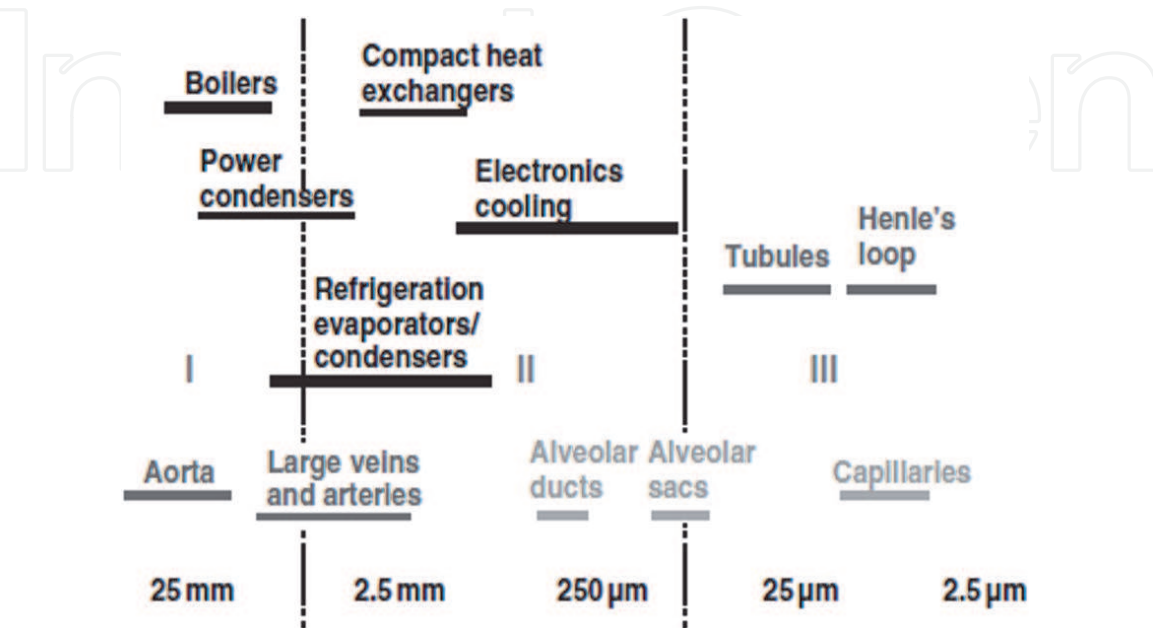
transfer enhancement was achieved as compared to the minichannel heat exchanger tested under the same conditions. The non-post processed surface of the DMLS manufactured microchannel is likely to be the main contributor to the augmented heat transfer performance. Further studies are required to fully appreciate the possible mechanisms behind this phenomenon as well as the convective heat transfer properties of nanoemulsion fluids.

Keywords: ethanol/polyalphaolefin nanoemulsion, minichannel, additively manufactured microchannel, single-phase flow, two-phase flow boiling, heat transfer enhancement

1. Introduction

Fluid flow within the channels can be viewed as the heart for plenty of natural and industrial systems. Heat and mass transfer are carried out along the walls of channels existing in biological systems, for instance blood vessels, kidney, lungs, and brain, as well as in many of industrial systems, for example heat exchangers, air separation plants, water desalination systems, and nuclear power reactors [1]. **Figure 1** illustrates a range of channel dimensions applied for different systems. While the smallest channel dimensions are observed in the biological systems undergoing mass transport, the larger dimensions are employed for the transportation of fluids. From a technological point of view, a steady transition from the larger channel dimensions, order of magnitudes of 10 to 25 mm, to the smaller channel dimeters, order of magnitudes of tens to hundreds of μm, can be seen in the recent years.

Generally, the energy transport process takes place along the channel wall, while the bulk flow occurs through the channel's cross-sectional area. The transport rate varies with the surface area, being in a linear proportion to the channel diameter (D), while the flow rate shows a direct proportion to the cross-sectional area (D^2). Hence, the ratio of channel surface area to the volume is proportional to 1/D. Obviously, a reduction in the channel diameter leads to the increase in the ratio of surface area to volume.

Figure 1.
Channel diameter ranges applied for different applications [2].

By shifting to the smaller channel dimensions, some of the conventional principles of fluid flow, mass transport, and energy transport need to undergo reevaluation for validation or possible revisions. The following three main reasons can be mentioned to address the difference in the fluid flow modeling between conventional and mini/microchannels [3]:

    i. some changes realized in the fundamental principles; as an illustration, the continuum hypothesis may not be valid for gas flows in mini/microchannels, or a deviation arisen from an enhanced effect of some forces (e.g., electrokinetic),

    ii. uncertainties originating in those factors extracted empirically from experiments on the large-size channels, for instance pressure loss coefficients of fluid flow at the tube entrance and exit,

    iii. uncertainties originating from microscale measurements, either in geometry or operating conditions.

In the heat transfer applications, the reasons which drive such a shift towards smaller flow passages are as follows [2]:

    i. Substantial enhancement of heat transfer,

    ii. Improved dissipation of heat flux in the microelectronic circuits and devices,

    iii. Development of micro-scale devices which require the equally small cooling systems.

The use of smaller channels provides a better performance in heat transfer, albeit accompanied mostly with an increase in the pressure drop. An optimal balance between these parameters results in the various channel dimensions for different applications. Take as an illustration, in automobile industry, the dimensions of flow passages in evaporators and radiators have reached to nearly 1 mm as a result of the balance between the cleanliness standards, heat transfer, and pumping power. Similarly, the high heat fluxes generated by microelectronic devices as well as the geometric and dimensional constraints imposed by the micro-scale devices and microelectromechanical systems (MEMS) require a drastic reduction in the dimensions of flow channels designed for their cooling systems. Also, the mirrors used for high-power laser devices employ the cooling systems having extremely small footprint. The continuous advances in the fields of genetic and biomedical engineering are contingent upon the precise transport control and thermal control of fluid flow in the micro-scale passages. Hence, a solid understanding of heat transfer process and fluid flow in such micro-scale systems is crucial to the design and operation.

1.1 Classification of flow channels

The hydraulic diameter can serve as an indicator for taking into account a channel's dimensions and then classifying the flow channels. The reduction in channel dimensions has different impacts on various processes. Although the derivation of particular criteria based on different process parameters seems to be fascinating, a simple dimensional-based classification is typically employed in the literature due to the abundance of process parameters arising in the transition from

conventional to micro dimensions. The channel classification suggested in [4] has categorized the range of 1–100 μm as the microchannels, 100 μm to 1 mm as the mesochannels, 1–6 mm as the compact passages, and the range above 6 mm as the conventional channels.

Kandlikar et al. [3] improved their channel classification reported earlier in [5], and then presented a more general classification according to the minimum channel dimension, shown in **Table 1**. In this table, D indicates the channel diameter. However, in case the channel is non-circular, the smallest channel dimension is recommended to be taken for D; for instance, in a rectangular channel the smaller side is considered for D. This channel classification may be used for either of single-phase or two-phase flow applications.

For the case of phase-change heat transfer in particular, the channels with various scales are classified according to the Bond number proposed by Cheng et al. [6] for expressing the transition from macroscale heat transfer to microscale heat transfer. Bond number takes into consideration the impacts of pressure, tempera-ture, and some thermophysical properties of a fluid and is given as follows:

$$Bo = \left(\frac{D_h}{l_C}\right)^2 \tag{1}$$

where D_h stands for hydraulic diameter, and l_C accounts for capillary length expressed as:

$$l_C = \sqrt{\frac{\sigma}{g\,(\rho_1 - \rho_V)}} \tag{2}$$

For water at 373 K, the capillary length (l_C) of water is practically 2.72 mm. Based on Cheng's et al. classification, the channels with the range of a hydraulic diameter (D_h) between 600 μm and 4,720 μm can be considered as minichannels for the applications using water as the base liquid. **Table 2** shows the channel classification based on Bond Number (Bo) for water at 373 K.

Channel Classification	Smallest Channel Dimension (D)
Conventional Channels	D ˃ 3 mm
Minichannels	3 mm ≥ D ˃ 200 μm
Microchannels	200 μm ≥ D ˃ 10 μm
Transitional Microchannels	10 μm ≥ D ˃ 1 μm
Transitional Nanochannels	1 μm ≥ D ˃ 0.1 μm
Nanochannels	0.1 μm ≥ D

Table 1.
Channel classification based on dimensions.

Channel Classification	Bond Number (Bo)	Hydraulic Diameter
Microchannels	Bo <0.05	D_h < 600 μm
Minichannels	0.05 < Bo <3	600 μm < D_h < 4720 μm
Macrochannels	Bo >3	D_h > 4720 μm

Table 2.
Channel classification based on bond number for water at 373 K.

In the present study, we follow and meet both the selection criteria stated above for channel classification (i.e., **Tables 1** and **2**) to ensure proper differentiation in performance between minichannels and microchannels as well as proper collection of the literature associated with heat transfer of mini and/or microchannels.

1.2 Ethanol/polyalphaolefin nanoemulsion: a novel heat transfer fluid

A variety of industries and military sectors have faced the challenge of finding effective and efficient thermal management solutions as the electronic systems used can output heat flux as high as 100 W/cm^2 [7–11]. While many advanced works have been performed to develop high performance heat exchangers with varieties of shape, size and tube surface augmentation, the bottleneck of improvement has fall into how to develop efficient heat transfer fluids with significantly improved thermal properties over those currently available. To date, several heat transfer fluid candidates have been reported, which include, but not limited to, nanofluids [12–34], dilute emulsion [35, 36], and emulsion [37–41]: Nanofluid has been intensively studied since it was proposed in 1995 by Choi [42]. It is consisted of a mixture of solid nanoparticles and base fluid, and it has been reported to be potentially useful in applications such as nuclear power system, solar collector, and compact high power density electronics system. Emulsion and dilute emulsion fluid are essentially similar systems made of a mixture of two immiscible liquids, while the "dilute emulsion" has 5 vol% or less dispersed component. Using emulsion to enhance heat transfer can be dated back to 1959 by Moore [43], and it has attracted interests of researchers [35–45]. One of the most detailed descriptions of how emulsions boil is the work of Bulanov and Gasanov [38–41, 44, 45], in which they proposed chain-reaction boiling of the droplets as an explanation for the observed superheated droplets and bubble dynamics on the heat surface. In addition, Rosele [46] et al. carried out an experimental study of boiling heat transfer from a horizontal heated wire, including visual observations in which the heat transfer could be enhanced in dilute emulsions compared to that of water as a base fluid.

Recently, the authors have proposed a new type of heat transfer fluid called "nanoemulsion" [47]. Nanoemulsion is a suspension of liquid nanodroplets formed by self-assembly inside another immiscible fluid, as part of a broad class of multiphase colloidal dispersions [48]. The nanoemulsion eliminates the presence of solid particles, which usually cause abrasion and erosion issues even with extremely fine particles such as nanoparticles [49–53], and instead, uses liquid nanostructures [54–63]. The droplets typically have a length scale less or equal to 50 nm, which makes the nanoemulsion fluid thermodynamically stable and transparent to natural light. A comparison of nanoemulsion with emulsion (dilute emulsion) is represented in **Table 3** [47, 48].

Property	Nanoemulsion	Emulsion
Appearance	Transparent	Turbid
Interfacial tension	Ultra-low ($<<$1 mN/m)	Low
Droplet size	<50 nm	>500 nm
Phase stability	Thermodynamically stable	Thermodynamically unstable
Preparation	Self-assembly	Need of external shear
Viscosity	Newtonian	Non-Newtonian

Table 3.
Comparison of Nanoemulsion and emulsion (dilute emulsion).

Pool boiling heat transfer studies of nanoemulsion fluids have shown that: (i) the thermophysical properties of the nanoemulsion fluids are found to be better than that of the base fluid [54, 55]; and (ii) an appreciable increase in heat transfer coefficient (HTC) and critical heat flux (CHF) can be observed in nanoemulsion fluids when the phase-changeable nanodroplets formed inside undergo nucleation [57, 61, 62].

Convective heat transfer of conventional heat transfer fluids inside mini/microchannel heat exchangers has been extensively studied due to its capability to remove high heat fluxes [33, 36, 64–66]. However, relatively few studies have been carried out to investigate the application of novel heat transfer fluids inside mini/microchannels. The recent development of nanotechnology has led to the improvement of heat transfer coefficient using novel nanostructured working fluids. While there are some recent experimental studies addressing the possibility of using nanostructured heat transfer fluids inside micro/nanostructured surface to enhance heat transfer [26, 31, 34], other recent studies showed that the use of nanofluids and nanotube coating offers a lower heat transfer coefficient at the coated surface compared to the bare surface [67–70].

Despite the significant enhancement observed in pool boiling heat transfer of nanoemulsion fluids compared to the base fluids, it remains inconclusive whether the same optimistic outlook can be expected in the convective heat transfer of nanoemulsion fluids. The present study aims to numerically and experimentally investigate the flow and heat transfer characteristics of ethanol/PAO nanoemulsion inside a conventionally manufactured minichannel and compares them with those of a microchannel heat exchanger manufactured additively.

2. Experimental approach

2.1 Preparation of nanoemulsion

To minimize the impact of the differences in thermophysical properties of the two constitutive fluids on the convective heat transfer experiments, ethanol and PAO fluids were used to prepare the nanoemulsion for this study since their thermal conductivity values are very similar. Dioctyl sulfosuccinate sodium salt (Sigma Aldrich) was used as a surfactant to form the nanoemulsion.
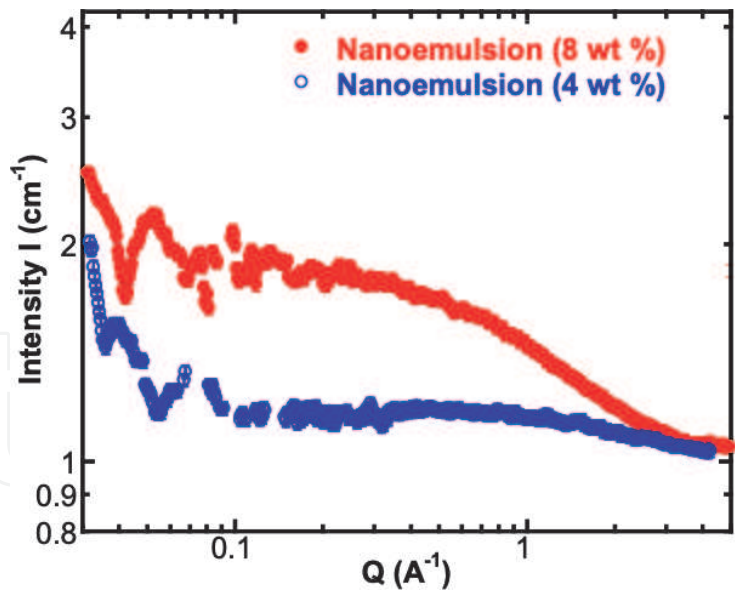
In the preparation process, the first step was to add the dioctyl sulfosuccinate sodium salt (Sigma Aldrich) into PAO fluid. The mixture was stirred until the dioctyl sulfosuccinate sodium salt was completely dissolved. The second step is to inject ethanol into the base fluid and mix them well until the mixture became transparent. In the present study, ethanol (4 or 8 percentage of ethanol by weight) is added into PAO to form 4 wt % or 8 wt % Ethanol/PAO nanoemulsion fluids respectively.
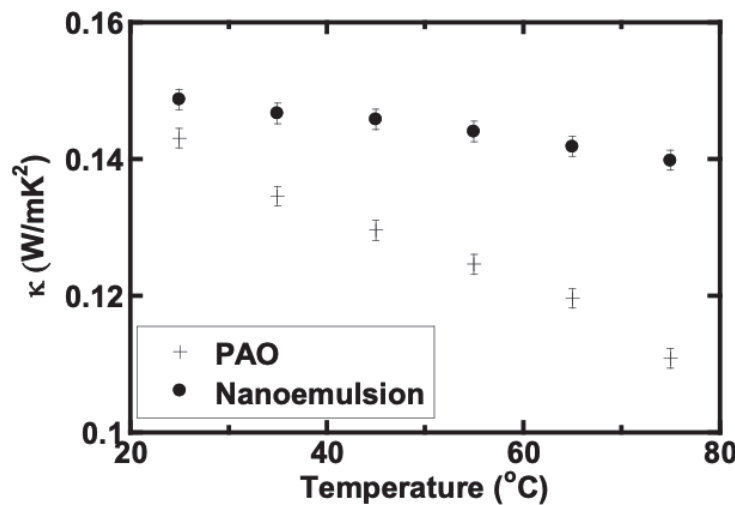
2.1.1 Structural properties

Figure 2 shows the small angle neutron scattering (SANS) experimental results of ethanol nanodroplets measured by NG7 SANS beamline at NIST Center for Neutron Research (NCNR), and the data was reduced to extract the structural information following the protocol provided by NCNR [71, 72]. It was found that the ethanol nanodroplets formed inside the nanoemulsion fluids have a radius of less than 1 nm on average.

2.1.2 Thermophysical properties

Thermal conductivity and viscosity are macroscopically observable parameters that affect the thermal performance of the fluids. **Figure 3** shows the thermal

Figure 2.
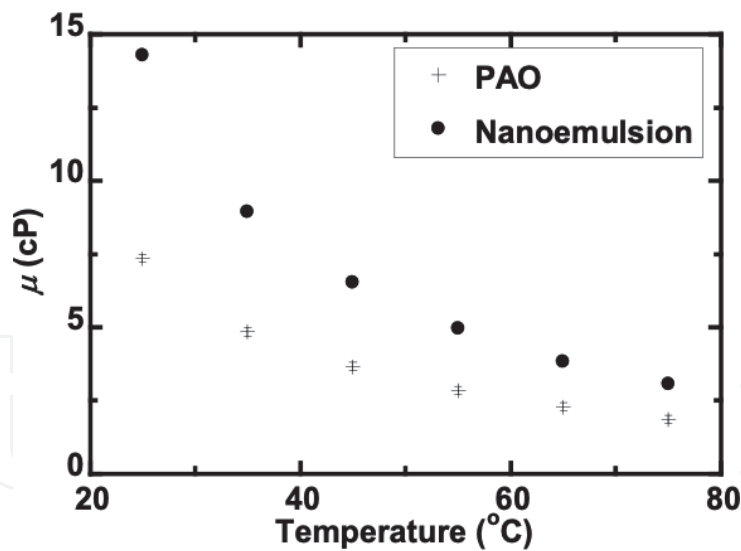*Small angle neutron scattering curves for 4 wt % and 8 wt % ethanol/PAO nanoemulsion heat transfer fluids.*

Figure 3.
Thermal conductivity of the pure PAO and 8 wt % ethanol/PAO nanoemulsion at temperature range of 25 ∼ 75°C.

conductivities of the base PAO fluid and 8 wt % Ethanol/PAO nanoemulsion fluid and their dependence upon temperature. Thermal conductivity of the pure PAO and Ethanol/PAO nanoemulsion fluids was measured in the temperature range from 25–75°C using the 3ω-wire method [56]. As represented in **Figure 3**, the Ethanol/PAO nanoemulsion fluid experimented here exhibits a higher thermal conductivity compared to pure PAO: a 3.9% increase which agrees well with the earlier study [57]. In addition, the thermal conductivity decreases with higher temperature but at a substantially lower rate compared to pure PAO.

Similarly, the viscosity of the Ethanol/PAO nanoemulsions was measured using a commercial viscometer (Brookfield DV-I Prime) from 25–75°C. In general, the viscosity is found to decrease with increasing temperature in most heat transfer fluids, which is also observed in the proposed Ethanol/PAO nanoemulsion, that is, a decrease from 14.3 cP to 3.05 cP as illustrated in **Figure 4**, which agrees well with the authors' previous study [57].

The thermophysical properties considered in the present study for ethanol/PAO nanoemulsion and pure PAO fluids to conduct experimental heat transfer tests are summarized in **Table 4**.
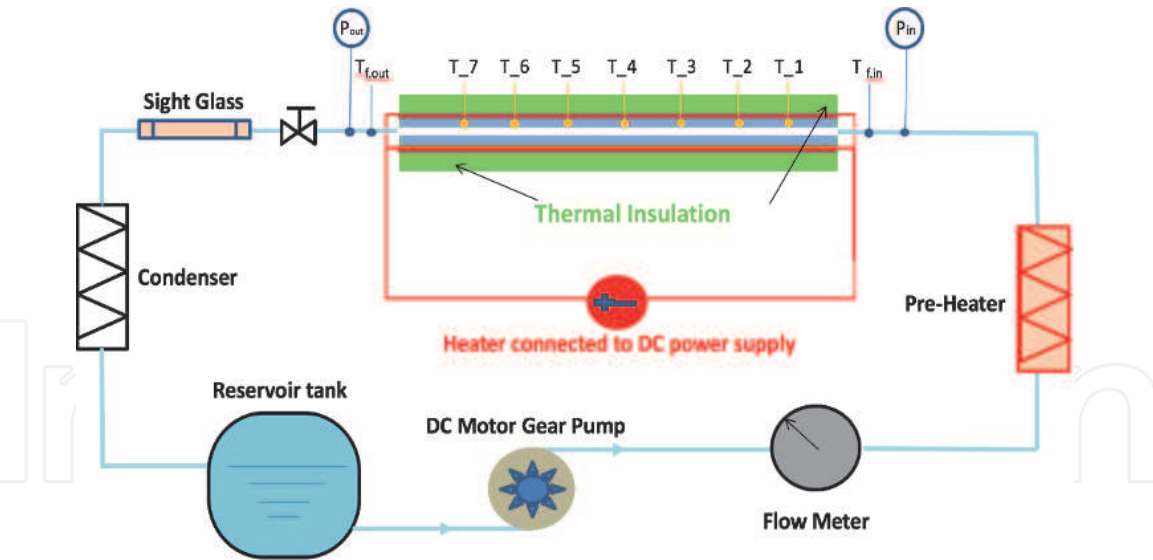
Figure 4.
Dynamic viscosity of the pure PAO and ethanol/PAO Nanoemulsion fluids at temperature range of 25 ∼ 75°C.

Property	4 wt % Nanoemulsion	8 wt % Nanoemulsion	PAO
Density (kg/m^3)	794	792	798
Conductivity (W/m-K)	0.148	0.149	0.143
Viscosity (kg/m-s)	13.8×10^{-3}	14.3×10^{-3}	7.34×10^{-3}
Nanodroplet radius (*nm*)	0.5	0.8	N/A

Table 4.
Thermophysical properties of ethanol/PAO Nanoemulsion and PAO at 25°C.
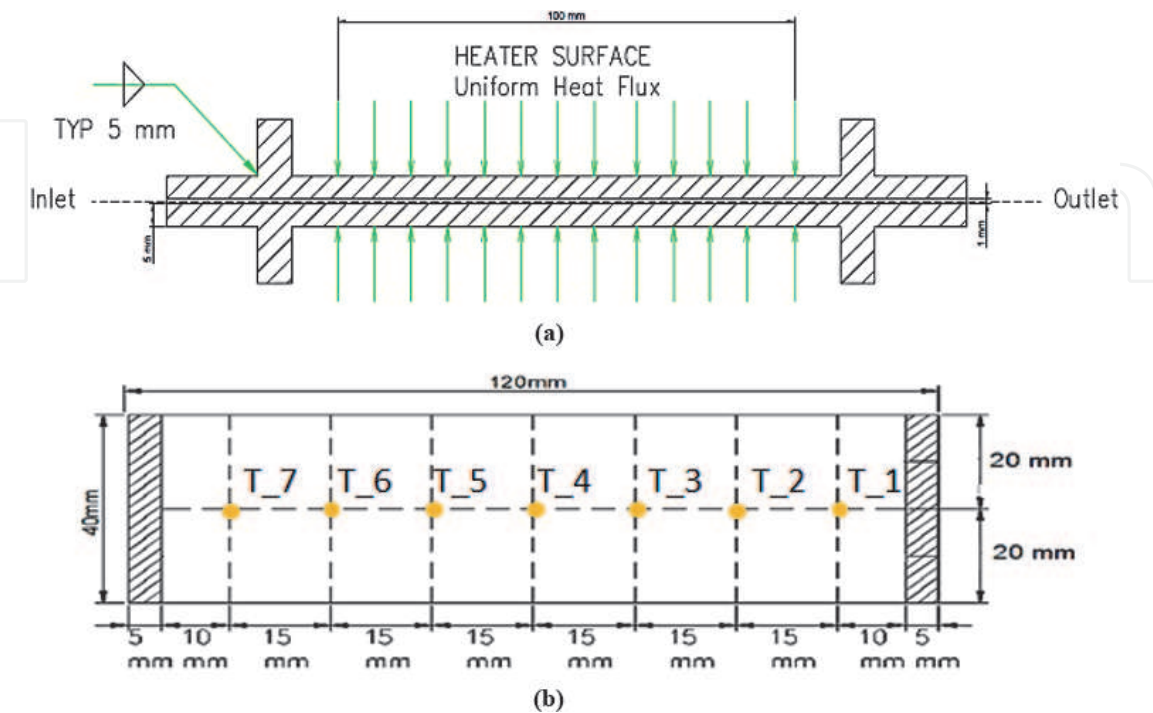
2.2 Experimental apparatus

The convective heat transfer tests of nanoemulsion fluids were carried out for two heat exchangers comprising a conventionally manufactured minichannel of 12 circular channels and an additively manufactured microchannel of 30 rectangular channels, both with the same exterior heat exchanger geometry. A schematic of the test loop setup built to conduct experiments is shown in **Figure 5**. The test apparatus consists mainly of a horizontal test section of either minichannel or microchannel heat exchanger, three gear pumps, a fluid reservoir, a flow sight glass, preheating section, condenser, and data acquisition system to measure and record the pressure, temperature, and mass flow rate. In the present study, the heat transfer tests were performed under a uniform wall heat flux applied on the top and bottom surfaces of the minichannel and microchannel heat exchangers. A programmable DC power supply with 0.05% power uncertainty was used to electrically heat up the test sections in order to obtain the constant wall heat flux. Furthermore, the preheating section was also electrically heated by a circulator, and the inlet fluid temperature is controlled at a desired value before entering the test sections. The inlet and outlet fluid temperatures were measured by two K-type thermocouples. The test section was carefully wrapped using an insulation material with a thermal conductivity of 0.043 $W/(m.K)$. A layer of aluminum foil was then wrapped on the outside of thermal insulation layer. The heat losses through the insulation layer were estimated to be lower than 2% of total heat losses and it was neglected in thermal performance calculations in the present study. Pressure drops of the test section were measured by two GP-50 differential pressure transducers with a working range of 0–200 kPa and an uncertainty of 0.25%. For all the tests conducted, both minichannel and

Figure 5.
Schematic of the test apparatus.

microchannel heat exchangers were placed horizontally to the ground. The liquid in the reservoir was first preheated to a preset temperature of 75°C. The liquid flow rate was adjusted to the desired value and monitored by a digital paddle wheel flow meter (Micro-Flow™). Within the experiments, the fluid temperature and surface temperature were automatically recorded by the data acquisition system. The test system reached steady-state conditions while the changing rates of all the set parameters mentioned above were less than 0.2%. The entire test rig was fully automated using the National Instrument LabVIEW software and data acquisition devices (National Instruments Corp., Austin, TX, USA).

Figure 6(a) and **(b)** depict the side-view and top-view of the test sections respectively, in which seven thermocouples were attached to the top surface of both minichannel and microchannel heat exchangers and were used to measure the local

Figure 6.
Schematic of the test sections (both mini- and microchannels): (a) side view, (b) top view with wall-mounted thermocouples.

Geometry					
Test Section	**Material**	**Cross Section**	**Orientation**	**Channel Diameter**	**Length**
Microchannel	316 L Steel	Rectangular	Horizontal	$640\mu m \times 760\mu m$	120 mm
Minichannel	Aluminum	Circular	Horizontal	1 mm	120 mm
Operating Conditions at Inlet of Test Sections					
Loop	Working Fluid	T_{in}	P_{in}	Heat Flux	Mass Flux
Single-Phase Flow	Nanoemulsion	75°C	159 kPa	13–44 kW/m²	1063–8504 Kg/m²-s
Two-Phase Flow	Nanoemulsion	75°C	159 kPa	13–44 kW/m²	630–5037 Kg/m²-s

Table 5.
Geometry of the test sections along with operating conditions used.

wall temperatures as shown in **Figure 6(b)** where each red dot represents one wall-mounted thermocouple.

Table 5 summarizes geometry of both test sections (minichannel and microchannel) coupled with the operating conditions applied to conduct experimental tests for single-phase flow and two-phase flow as well as to conduct numerical analysis of heat transfer performance for comparison purposes.

2.2.1 Data processing

In the present study, the average heat transfer coefficient *h* is used and expressed as follows:

$$h = \frac{q_{wall}}{T_s - T_f} \tag{3}$$

where q_{wall} is the local heat flux estimated by considering the local heat loss as shown in Eqs. (4) and (5) for minichannel and microchannel respectively, T_s is the average local surface temperature measured by the wall-mounted thermocouples along the channel direction calculated by Eq. (6), T_f is the fluid's bulk mean temperature calculated by Eq. (7).

$$q_{wall} = \frac{Q}{n(\pi DL)} \tag{4}$$

$$q_{wall} = \frac{Q}{n(2HL + 2WL)} \tag{5}$$

$$T_s = \frac{1}{7}\sum_{x=1}^{x=7} T_x \tag{6}$$

$$T_f = \frac{1}{2}\left(T_{f,in} + T_{f,out}\right) \tag{7}$$

The average Nusselt number of nanoemulsion fluid can be expressed by:

$$Nu = \frac{h\,D_h}{k_f} \tag{8}$$

in which D_h is the hydrodynamic diameter for either of minichannel or microchannel.

The Reynolds number of the flow can also be calculated as follows:

$$Re = \frac{\rho V D}{\mu} \tag{9}$$

Total pressure loss along the test sections is calculated by:

$$\Delta P = \Delta P_{friction} + \Delta P_{minor} \tag{10}$$

and the friction factor is calculated by:

$$f = \Delta P_{friction} \frac{2D}{\rho L V^2} \tag{11}$$

To take the shape of the channel's cross-section into consideration, the Poiseuille number (Po) can be found to be only a function of microchannel's aspect ratio:

$$Po = f \times Re = \frac{4\pi^2(1 + \varepsilon^2)}{3\sqrt{\varepsilon}(1 + \varepsilon)} \tag{12}$$

in which $\varepsilon = H/W$.

2.2.2 Uncertainty propagation

The uncertainties for different parameters involved in the experimental tests are listed in **Table 6**.

An uncertainty analysis is performed from the measurement uncertainties using calculus and the principle of superposition of errors. In general, for a variable F that is a function of several variables such as $F = F(a, b, c, ...)$, the squares of the

Parameter	Uncertainty
Temperature (°C)	±0.1
Flow velocity (m/s)	±6%
Position of the thermocouples (m)	±0.01
Dimensions of the minichannel (m)	±0.002
Dimensions of the microchannel (m)	±0.002
Power input (W)	±0.5%
Heat flux (W/m^2)	±0.5%
Pressure (Pascal)	±0.25%

Table 6.
Uncertainties sources for the experimental tests.

Calculated Variable	Uncertainty
Heat transfer coefficient, h	±6%
Nusselt number, Nu	±8%
Reynolds number, Re	±6%
Friction factor, f	±10%

Table 7.
Uncertainties for heat transfer performance parameters.

uncertainty in F is the sum of the square of the uncertainties due to each independent variable, $\delta F = \left[\left(\frac{\partial F}{\partial a} \delta a \right)^2 + \left(\frac{\partial F}{\partial b} \delta b \right)^2 + \left(\frac{\partial F}{\partial c} \delta c \right)^2 + ... \right]^{0.5}$ where δa stands for the uncertainty due to variable a. The uncertainties of the heat transfer performance parameters are calculated and represented in **Table 7**.

3. Conventionally manufactured minichannel heat exchanger

Figure 7 illustrates the minichannel heat exchanger of 12 circular channels designed and fabricated conventionally to conduct the experimental tests. The material and geometry of the minichannel test section was shown earlier in **Table 5**, coupled with the operating conditions engaged to run the experiments.

Using the PAO base fluid, the flow and heat transfer characteristics of the minichannel test section were carefully evaluated to verify the integrity of the experimental facility and test procedures. The experiments on the PAO base fluid were first performed, and the test results were used as baseline data to compare with those of Ethanol/PAO nanoemulsion fluids of 4% and 8% wt% ethanol. A range of heat fluxes addressed earlier in **Table 3** was selected as heat inputs to simulate single-phase and two-phase flow heat transfer conditions. All the experiments performed in the present study were repeated five times, and the relative errors of test data were found to be less than 5%. The SANS measurements were performed on the samples only prior to initiating the experiments. However, previous studies on a similar water/PAO system have demonstrated that there are no remarkable structure changes of the nanodroplets before and after pool boiling tests inside an enclosed system [63].

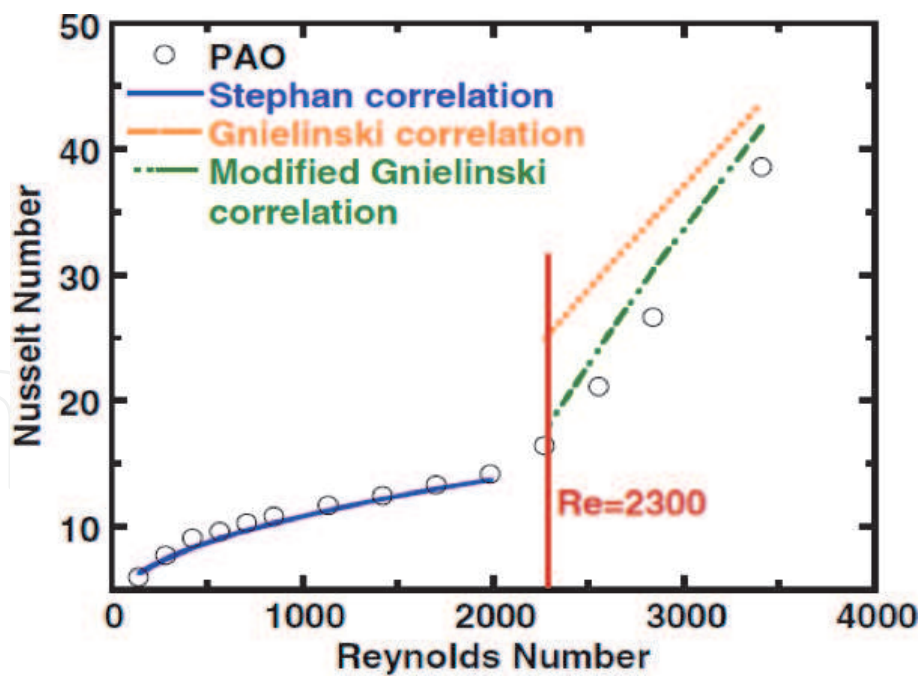### 3.1 Results and discussions

3.1.1 Experimental results

3.1.1.1 Single-phase results of PAO Base fluid

Figure 8 illustrates variations of average Nusselt number with Reynolds for the pure PAO base fluid and compares the results with the empirical heat transfer correlations tabulated in **Table 8**. While Stephan correlation was used to predict

Figure 7.
Traditionally manufactured minichannel heat exchanger developed for the present comparative study.
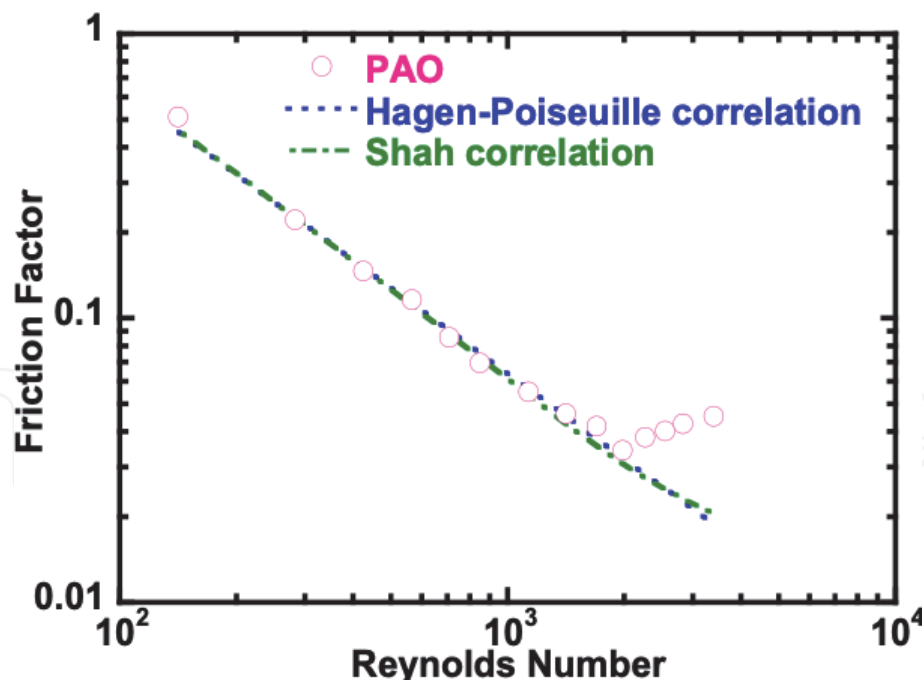
Figure 8.
Average Nusselt number versus Reynolds number for pure PAO fluid.

Correlation	Conditions	Validity Range
Stephan correlation [73] $Nu = 4.364 + \dfrac{0.086\left(RePr\frac{D}{L}\right)^{1.33}}{1+0.1Pr\left(Re\frac{D}{L}\right)^{0.83}}$	Laminar flow in a circular pipe	$Re < 2300$
Gnielinski correlation [73] $Nu = \dfrac{(\,f/8)(Re-1000)Pr}{1+12.7\sqrt{\frac{f}{8}}\left(Pr^{\frac{2}{3}}-1\right)}$ where $f = \dfrac{1}{(1.82\log(Re)-1.64)^2}$	Constant wall heat flux, fully developed turbulent and transitional flow	$3000 < Re < 5 \times 10^4$
Modified Gnielinski correlation [74] $Nu = \dfrac{(\,f/8)(Re-1000)Pr}{1+12.7\sqrt{\frac{f}{8}}\left(Pr^{\frac{2}{3}}-1\right)}$ where $f = 3.03 \times 10^{-12} \bullet Re^3 - 3.67 \times 10^{-8} \bullet Re^2 + 1.46 \times 10^{-4} \bullet Re - 0.151$	Constant wall heat flux, transitional flow in a straight circular pipe	$2300 < Re < 4500$

Table 8.
Empirical heat transfer correlations used for comparison purposes with their validity ranges.

heat transfer characteristics within the laminar regime [73], the Gnielinski correlation was exploited for fully developed turbulent flow regime [73] and modified Gnielinski correlation [74] was used for comparison purposes within the transitional flow regime. As shown by the measured data and empirical correlations in **Figure 8**, the Nusselt number consistently increases with the Reynolds number, however it starts to increase at a greater rate for Reynolds greater than 2300 (critical Reynolds), which indicates a transition from laminar to turbulent flow regime. As represented in this figure, the experimental heat transfer results show good agreements with the empirical correlations in both laminar and transitional flow regimes.

Figure 9 shows variations of friction factor with Reynolds number for the pure PAO base fluid and compares the results with the empirical friction factor correlations listed in **Table 9**. The Hagen-Poiseuille correlation was used to predict flow characteristics within the fully developed laminar flow regime inside a circular minichannel [73] whereas the Shah correlation was used to include the entrance effect within the hydrodynamically developing region [73]. As represented in

Figure 9.
Friction factor versus Reynolds number for pure PAO fluid.

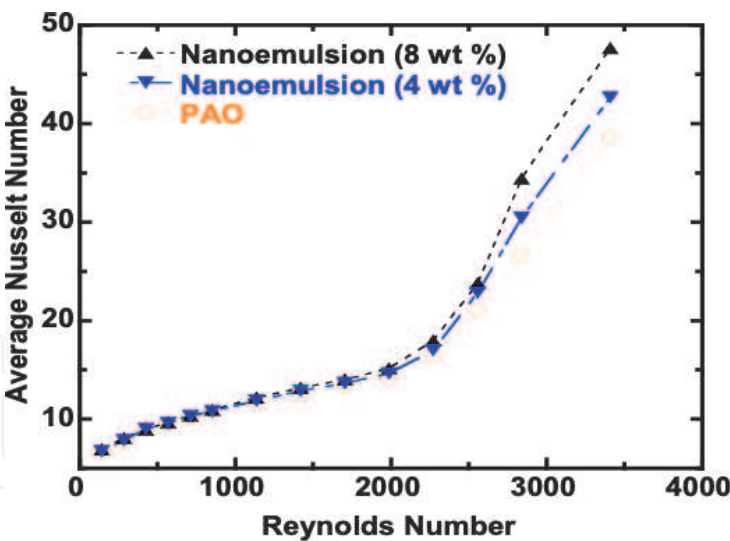| Correlation	Conditions	Validity Range
Hagen-Poiseuille correlation [73] $f \bullet Re = 64$	Laminar flow in a circular channel	$Re < 2300$
Shah correlation [73] $f \bullet Re \approx 4 \left(\frac{3.44}{\sqrt{\xi}} + \frac{16 + 0.3125\xi - \frac{3.44}{\sqrt{\xi}}}{1 + 2.12 \times \frac{10^{-4}}{\xi^2}} \right)$ where $\xi = \left(\frac{x}{D} \right) / Re$	Laminar flow inside circular channel with consideration of entrance length	$Re < 2300$

Table 9.
Empirical friction factor correlations used for comparison purposes with their validity ranges.

Figure 9, the measured values of friction factor for the pure PAO flowing inside the minichannel agree well with the empirical correlations during laminar flow regime. The friction factor decreases when Reynolds number increases up to around 2000. Afterwards, the friction factor starts to increase sharply for Reynolds greater than 2000, which indicates transition from laminar to turbulent flow regime.

3.1.1.2 Single-phase results of ethanol/PAO nanoemulsions

After confirming the integrity of the test loop using the experimental results of pure PAO fluid, heat transfer and flow characteristics of Ethanol/PAO nanoemulsion fluids with 4 and 8 wt% ethanol were experimentally investigated by following a similar test procedure.
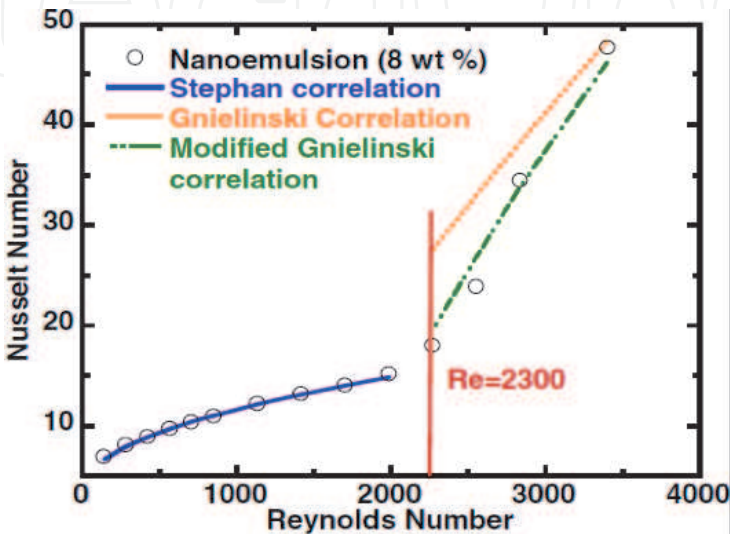
Figure 10 represents variations of average Nusselt for the base fluid and nanoemulsion fluids against a range of Reynolds lying in the laminar and transitional flow regimes. As shown in this figure, Nusselt increases with Reynolds for all the working fluids tested in the present study within either laminar regime (Re < 2300) or transitional regime (Re > 2300). **Figure 10** also illustrates that increase in ethanol concentration of nanoemulsion fluids does not reflect a remarkable distinction in heat transfer performance within the laminar regime. However, when ethanol concentration of nanoemulsions increases from pure PAO (0%) to 8 wt% nanoemulsion, Nusselt number exhibits significant enhancements within the

Figure 10.
Nusselt number versus Reynolds for pure PAO and nanoemulsion fluids.

transitional and the early stage of turbulent flow regimes. The results show a 24% increase in average Nusselt number for 8 wt% nanoemulsion fluid and a 11% increase in average Nusselt for 4 wt% nanoemulsion fluid compared to that of pure PAO at the same Reynolds number of 3400. The heat transfer enhancement in the transitional regime can be attributed to the enhanced interaction and interfacial thermal transport between ethanol nanodroplets and PAO base fluid, so that the increase in density and size of nanodroplets at higher concentrations of ethanol can contribute to a stronger mixing and mass exchange effects within the transitional and turbulent flow regimes.

Figure 11 compares experimental heat transfer data for 8 wt% ethanol/PAO nanoemulsion with conventional heat transfer correlations suggested in the literature for internal flow. As shown in this figure, the experimental results agree very well with those predicted by the empirical correlations in both laminar and transitional flow regimes. While the classical Gnielinski correlation overestimates the Nusselt number for the transitional flow, the Stephan and modified Gnielinski correlations provide a better prediction of Nusselt number for the laminar and transitional flow regimes, respectively.
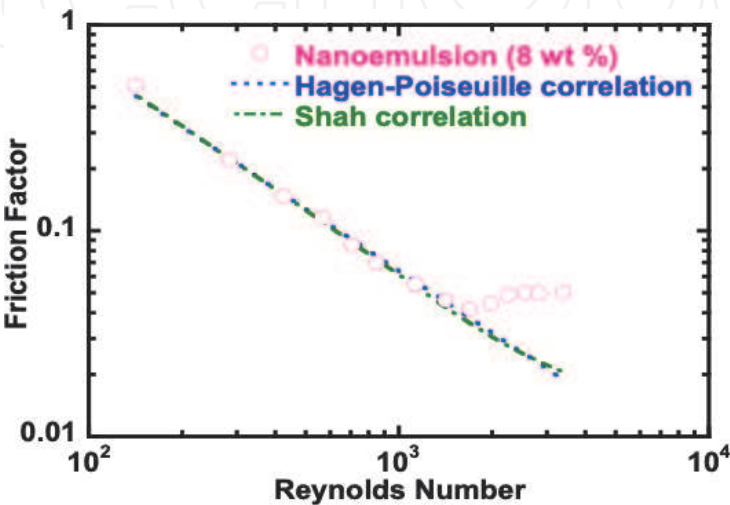

Figure 11.
Nusselt number versus Reynolds for 8 wt% ethanol/PAO nanoemulsion.

Figure 12 represents variations of friction factor with Reynolds number for 8 wt % ethanol/PAO nanoemulsion, and compares the experimental results with those predicted by the empirical correlations, in which a very similar trend can be observed with that of the single-phase PAO base fluid as previously shown in **Figure 9**. As illustrated in **Figure 12**, the friction factor of nanoemulsion within the laminar regime decreases consistently with Reynolds number up to the Reynolds of 2000, indicating a slightly earlier entrance into the transitional flow regime compared to that of the pure PAO. Upon entering the transitional regime, friction factor is found to increase and then starts to flat out at Reynolds number of around 3000. As clearly seen in this figure, the experimental data measured for friction factor of nanoemulsion showed good agreements with those predicted by the Hagen-Poiseuille and Shah correlations.

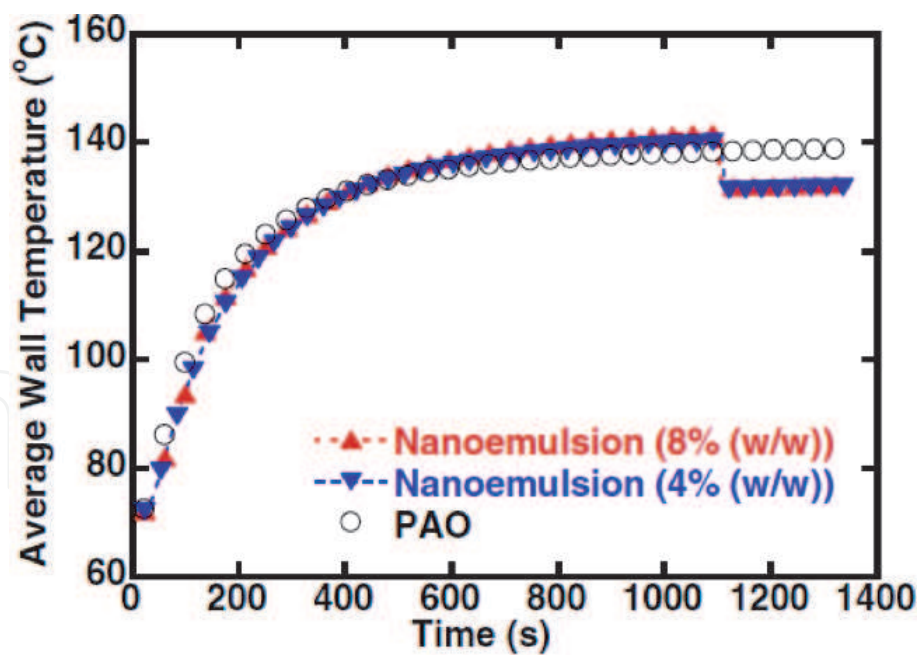### 3.1.1.3 Two-phase results of ethanol/PAO nanoemulsions

One of the reasons to replace conventional heat transfer fluids with nanoemulsion is to achieve significant heat transfer enhancements when the phase changeable nanodroplets undergo nucleation. Previous studies have demonstrated a significantly improved heat transfer coefficient and critical heat flux using nanoemulsion with phase changeable nanodroplets undergoing the nucleate boiling [57, 61, 62]. In the present study, the ethanol nanodroplets formed inside the nanoemulsion are expected to function as phase change nuclei at elevated temperatures during the two-phase flow boiling experiments. The maximum flow rate needs to be limited to less than 4.46 m/s (or Re = 1136) to maintain a wall temperature high enough to trigger flow boiling. Accordingly, all the flow boiling data collected and shown in the present study reflect heat transfer behavior within the laminar flow regime.

Figure 13 represents the variations of average transient wall temperature data for all the tested working fluids (4 and 8 wt% ethanol/PAO nanoemulsions and pure PAO) with time, which overlapped well with each other within single-phase flow regime. However, the wall temperatures of nanoemulsions started to deviate from the single-phase trend line, followed by a sudden drop in the wall temperature which indicates an increase in heat transfer coefficients due to the flow boiling. Using the sight flow indicator located next to the outlet of the minichannel test section, it was observed that there were bubbles coming out of the minichannel heat exchanger, which confirms that the ethanol nanodroplets underwent nucleation

Figure 12.
Friction factor versus Reynolds number (Nanoemulsion fluid).

Figure 13.
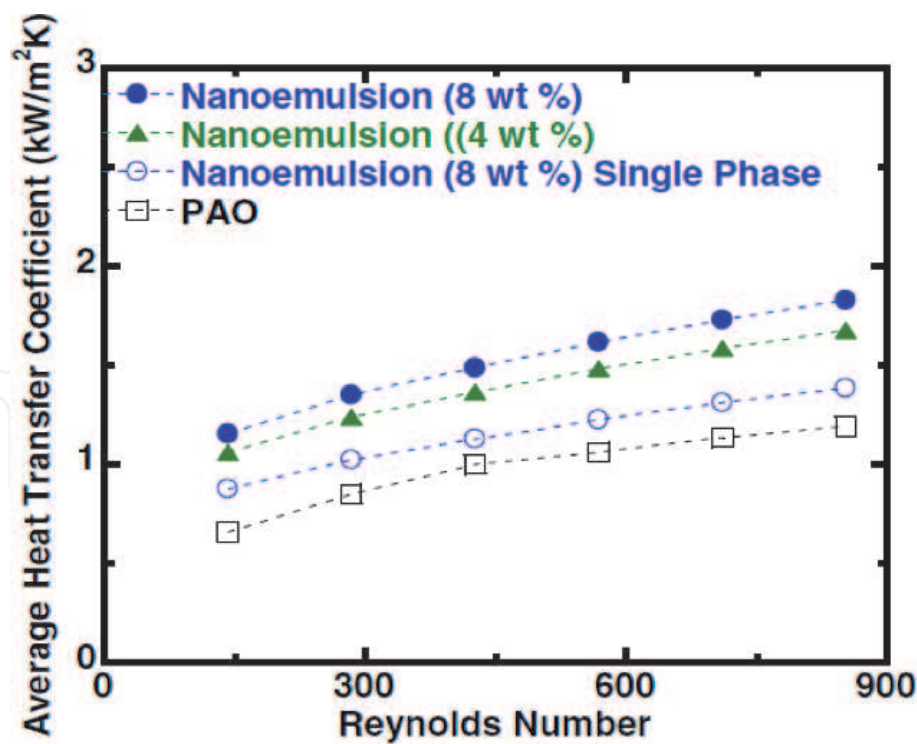*Evolution of the average wall temperature with time for pure PAO and nanoemulsions.*

and the flow lies in the state of two-phase flow boiling. Another interesting observation was the delay in nucleation boiling temperature or the onset of nucleate boiling (ONB). As illustrated in **Figure 13**, the nucleation did not start until the average surface temperature of the minichannels reached a temperature around 140°C while the boiling temperature for ethanol is 78°C. Similar findings of delayed ONB were previously reported for pool boiling experiments of sub-cooled ethanol/PAO nanoemulsion fluids [57]. The delayed ONB can be attributed to the inefficient thermal transport between each surfactant molecule and its surrounding PAO fluid, in which the PAO molecules are not packed closely near the hydrophilic head-group of the surfactant molecule and could not provide efficient thermal pathway in between the micelles and base fluid [59, 60].

Figure 14 shows the variations of average heat transfer coefficient with Reynolds number for flow boiling of nanoemulsion fluids, and compares them with those of single-phase flow of pure PAO and nanoemulsions. In addition to the fact that the Ethanol/PAO nanoemulsion fluids exhibit slightly higher heat transfer coefficients (HTCs) compared to those of pure PAO in single-phase flow due to the minor improvement in thermophysical properties, the HTCs were found to be significantly enhanced when the nanoemulsion fluids underwent two-phase flow boiling. It is also apparent that the phase change of the ethanol nanodroplets is the main contributor to the heat transfer improvement. **Figure 14** also reveals that the ethanol concentration of nanoemulsion has a positive impact on the overall heat transfer coefficients in both single-phase flow and two-phase flow boiling. As shown in this figure, an average HTC enhancement of 50 ∼ 70% was achieved with Ethanol/PAO nanoemulsion compared to that of the PAO base fluid.

3.1.2 Simulation results

The prototype of the minichannel heat exchanger was designed using CREO software and then the model was imported to COMSOL-Multiphysics to conduct numerical heat transfer analysis for the same geometry and operating conditions summarized in **Table 5**. The following assumptions were adopted to conduct the simulations: no slip boundary condition, normal inflow velocity, uniform wall heat

Figure 14.
Average heat transfer coefficient versus Reynolds for single-phase and two-phase flow of the working fluids.
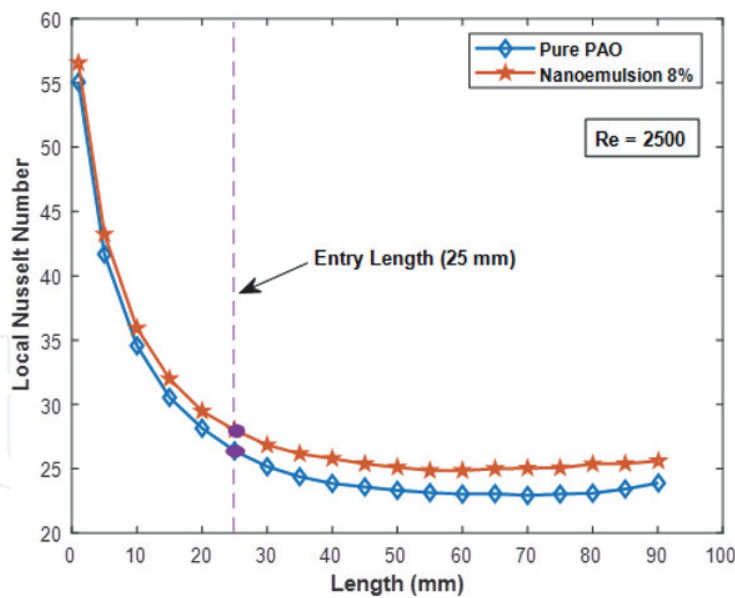
flux boundary conditions imposed on the top and bottom surfaces of the minichannel heat exchanger, and thermophysical properties of the working fluids are set to remain constant for the values addressed earlier in **Table 4**.

Three types of meshes were developed in the present study to examine accuracy of simulation results as well as to confirm mesh independency of the results, including finer, fine, and normal. The size settings for each mesh are shown in **Table 10**. The finer mesh size was eventually chosen as it allows to conduct sufficiently accurate analysis while still maintaining a reasonable computational time.

Figure 15 represents the variations of local Nusselt number at a certain Reynolds number of 2500 (i.e., the beginning of transitional regime) along the minichannel heat exchanger with the same geometry and dimensions used previously for the experimental investigations as summarized in **Table 5**. As illustrated in this figure, the local Nusselt number decreases along the minichannel at early positions and then reaches relatively constant values of 23 and 26 for the pure PAO and 8 wt%

Description	Finer	Fine	Normal
Calibrate for	Fluid dynamics	Fluid dynamics	Fluid dynamics
Maximum element size	0.148	0.212	0.4
Minimum element size	0.016	0.04	0.12
Curvature factor	0.4	0.5	0.7
Resolution of narrow regions	0.95	0.8	0.7
Maximum element growth rate	1.08	1.13	1.4
Number of elements	684,571	200,829	86,383
Mesh shape	Triangle	Triangle	Triangle
Computational time	14 min 25 sec	3 min 19 sec	1 min 22 sec

Table 10.
Mesh types developed to conduct numerical analysis.

Figure 15.
Variations of local Nusselt number along the minichannel at Re = 2500 for pure PAO and 8% ethanol/PAO nanoemulsion fluids with the entrance effects

Ethanol/PAO nanoemulsion, respectively, within the fully developed transitional region. This reveals a heat transfer enhancement of around 13% at a certain Reynolds number of 2500 using the 8 wt% nanoemulsion fluid compared to that of the pure PAO inside the minichannel heat exchanger.

This is important to point out that while the simulation results in **Figure 15** show the Nusselt values of 23 and 26 for the fully developed flows of pure PAO and 8% nanoemulsion, respectively, the experimental results of pure PAO and 8% nanoemulsion introduced earlier in **Figures 8** and **11** show the Nusselt values of around 21 and 24 at the same Reynolds of 2500, respectively. This indicates a relative deviation of approximately 9% between the model and experimental results.

As also observed from the simulation results in **Figure 15**, there is a declining trend of Nusselt number along the early locations of the minichannel. The significantly higher Nusselt number at the early locations and its subsequent sharp drop is due to the thermal entrance region at the inlet of the minichannel test section where the internal liquid single-phase flows are still neither thermally nor hydrodynamically fully developed. As a result of having a thermally developing flow in the entrance region, the thermal boundary layer is extremely thin which causes larger values of Nusselt and HTC compared to those of locations outside the entrance region where both of the working fluids are fully developed.

The hydrodynamic ($x_{fd,hyd}$) and thermal ($x_{fd,th}$) entry lengths for an internal flow in a circular channel can be calculated as follows, respectively [73]:

$$\frac{x_{fd,hyd}}{D} \approx 0.05 \, Re_D \tag{13}$$

$$\frac{x_{fd,th}}{D} \approx 0.05 \, Re_D Pr \tag{14}$$

The hydrodynamic entry length for the transitional flows of PAO and 8% nanoemulsion in the minichannel was found to be 25 mm. As demonstrated in **Figure 15**, the local Nusselt numbers for each of the working fluids take relatively constant values after the entry length of 25 mm where the boundary layer develops fully across the cross section of the microchannel and appears to be independent of

the channel length. Since the working fluids are PAO and nanoemulsion with Prandtl numbers greater than 1 (Pr > 1), the hydrodynamic boundary layer develops more quickly than the thermal boundary layer $\left(x_{fd,th} > x_{fd,hyd} \right)$.

4. Additively manufactured microchannel heat exchanger

4.1 Additive manufacturing of microchannel prototype

While micro- and minichannels show promising potential and have been incorporated in a wide variety of unique, compact, and efficient cooling applications, manufacturing of micro- and minichannels made of high temperature alloys is still a challenging task. Recently, additive manufacturing (AM) technology has shown its promising application in manufacturing [75–79]. The use of additive manufacturing, or widely known as 3D printing technique, has revolutionized the traditional manufacturing process, which now eliminates the traditional constrictions in geometry design and manufacturability. AM based manufacturing technique has opened the design potential of traditionally impossible geometries and structures.

The metal based additive manufacturing techniques, including: Selective Laser Melting (SLM), Selective Laser Sintering (SLS), and Electron Beam Melting (EBM), are the most widely studied. Of the aforementioned techniques, Direct Metal Laser Sintering (DMLS) method, as a subset of the SLS process, is particularly appropriate for building production-grade parts due to its ability to use high temperature alloys in the process [77, 80–83].

With DMLS, thin layers of atomized fine metal powder are evenly distributed using a coating mechanism onto a substrate plate, usually metal, that is fastened to an indexing table that moves in the vertical (Z) axis. This takes place inside a chamber containing a tightly controlled atmosphere of inert gas, either argon or nitrogen at oxygen levels below 500 parts per million. Once each layer has been distributed, each 2D slice of the part geometry is fused by selectively melting the powder. This is accomplished with a high-power laser beam, usually an ytterbium fiber laser with hundreds of watts. The laser beam is directed in the X and Y directions with two high frequency scanning mirrors. The laser energy is intense enough to permit full melting (welding) of the particles to form solid metal. The process is repeated layer after layer until the part is complete.

One of the unique characteristics of DMLS manufacturing process is that the surfaces of manufactured parts are intrinsically rough due to the nature of laser sintering process [80]. While the outward-facing surfaces can be smoothed via machining, internal surfaces cannot be post-processed easily. Stimpson et al. examined the effects of surface roughness on flow structures in DMLS parts containing microchannels [84]. In another study, Snyder et al. [85] analyzed the effect of building direction on flow structures in similar DMLS parts, paying particular attention to the different roughness features generated by different printing orientations. The authors of both studies [84, 85] reported relative roughness values ranging between 20% and 38% of the channel hydraulic diameters and proved that correlations for friction factor and heat transfer are no longer valid for surfaces with such high roughness values. Thus, it is imperative to characterize the internal surface of DMLS manufactured parts.

Many investigations have also been conducted to study flow behavior in microchannels of different cross-sections such as rectangular, circular, trapezoidal, triangular, and elliptical [86–88]. Rectangular and trapezoidal cross-sections have been extensively studied for a wide range of applications, mainly due to practical considerations such as fabrication techniques, cost, and ease of manufacturing.

Most researchers have employed rectangular cross-sections for studying friction and pressure drop in microchannels. Since microchannels length is normally long (compared to other dimensions), inlet and exit effects have been neglected in most works.

In the present study, the additively manufactured microchannel heat exchanger was developed using the EOSINT M280 machine at the University of the District of Columbia (UDC). The machine takes advantage of the DMLS technique to 3D print the designed prototype. **Figure 16** represents the EOSINT M280 machine which can be used to seamlessly manufacture complex heat exchanger designs. The process parameters (material scaling, layer thickness, and beam offset) applied to the machine are listed in **Table 11**. Adjusting process parameters and investigating different building directions to understand their impacts on the prototype performance is beyond the scope of this study.

Using the aforementioned fabrication process, a rectangular cross-sectional microchannel heat exchanger was designed and additively manufactured with 316 L Stainless Steel. Each channel is designed to be $640 \mu m$ in width and $760 \mu m$ in height, with a length of 120 mm. A total of 30 microchannels were fabricated along the center of the heat exchanger. Flanges were manufactured on each end of the heat exchanger to fit the existing test loop and facilitate the experimental investigations. **Figure 17** represents the additively manufactured microchannel heat exchanger developed for the present study.
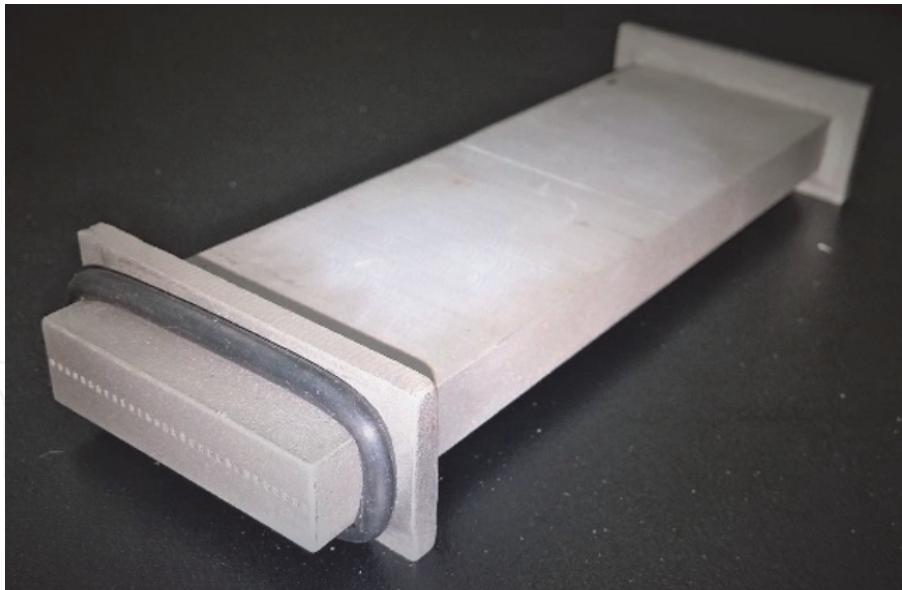

Figure 16.
EOSINT M280 machine used to develop the microchannel prototype.

Parameter	Setting
Material	316 L Stainless Steel
Process Gas	Nitrogen
Laser Power	400 W
Material Scaling X	0.045%
Material Scaling Y	0.16%
Beam Offset	0.11 mm
Layer Thickness	40 micrometer
Software	EOSTATE Magics RP (materialize)

Table 11.
Settings applied to EOSINT M280 machine to develop the prototype.

Figure 17.
Additively manufactured (AM) microchannel heat exchanger developed for the present study.

To characterize internal surfaces of the part including the roughness of each surfaces and true cross-section area, a computed X-ray tomography (CT Scan) was used. The CT scan takes a series of 2D images of an object and then incorporates them to form a 3D reconstruction of the object using the software algorithms. Through this method, the external and internal surfaces can be determined along with the channel surface roughness. An arithmetic roughness average, R_a, was calculated using the height differences between the CT scan data and the designed channel wall surface. The results have shown that the R_a/D_h value is 0.23.
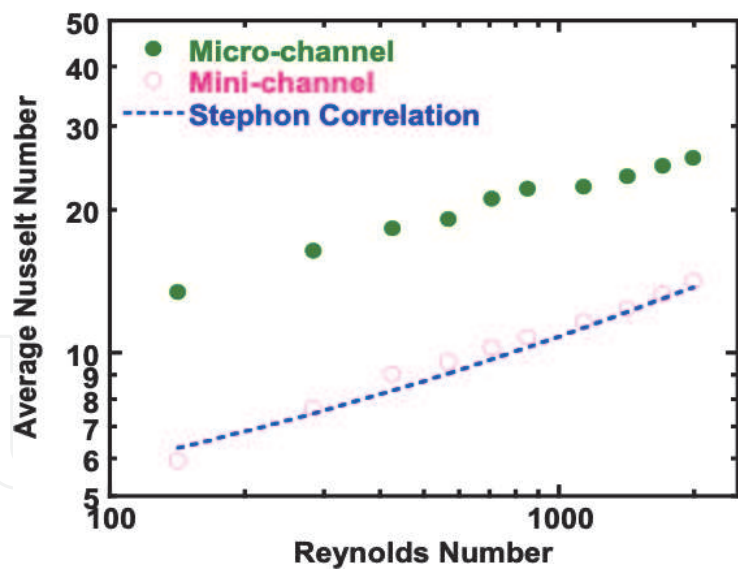
4.2 Results and discussions

4.2.1 Experimental results

After verifying the integrity of the experimental configuration and test procedures, heat transfer and flow characteristics of the single-phase flow of pure PAO fluid inside the additively manufactured microchannel were experimentally investigated and then compared with those of minichannel heat exchanger introduced earlier. All the experiments conducted in the present study were repeated five times, and the relative errors of test data were found to be less than 5%. Since Poisueille number remains constant with variations of Reynolds in the laminar regime, the experimental data for each set was averaged over the laminar flow regime.

Figure 18 represents the variations of the measured average Nusselt number with Reynolds for single-phase flow of the pure PAO within the laminar regime (100 < Re < 2000) for both microchannel and minichannel heat exchangers. As shown in this figure, while the Nusselt number gradually increases with Reynolds for both microchannel and minichannel, a significant enhancement of heat transfer is observed using the microchannel compared to the minichannel heat exchanger under the same operating conditions. Furthermore, the experimental results were compared with the Stephon's correlation for internal flow. As illustrated in **Figure 18**, the Stephon's correlation underestimates the Nusselt number inside the microchannel whereas it agrees well with the minichannel. The main reason for the reflected deviation is attributed to the larger surface roughness of the additively manufactured microchannel using the DMLS technique compared to that of the
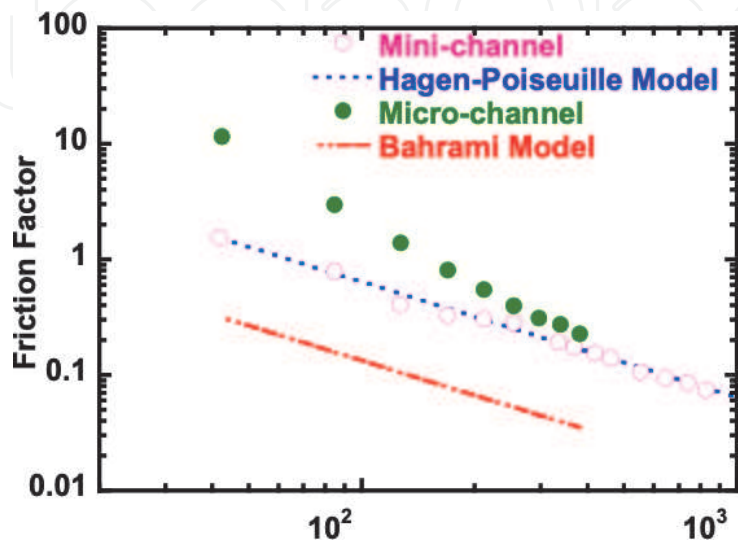
Figure 18.
Average Nusselt number versus Reynolds for the pure PAO fluid in both minichannel and microchannel heat exchangers.

traditionally manufactured minichannel heat exchanger. Stimpson et al. [84] and Snyder et al. [85] have investigated the effects of surface roughness and printing orientation on flow structures in DMLS manufactured parts and proved that the existing empirical correlations for heat transfer and friction factor are no longer valid for the additively fabricated surfaces with high roughness values. This is also important to point out that the non-post processed surface of the DMLS manufactured microchannels is likely to be the main contributor to the augmented heat transfer performance. Future study is then required to better appreciate the possible mechanisms behind the phenomenon observed here.

Figure 19 shows the variations of friction factor with a range of Reynolds numbers lying in the laminar regime for both the minichannel and microchannel heat exchangers. As clearly represented in this figure, the friction factor decreases with the increase of Reynolds number for both the test sections experimented in the present study. It can also be observed that the average friction factor of the PAO fluid inside the AM microchannel remains noticeably higher compared to that of the minichannel, and the entrance effect is more pronounced at lower Reynolds
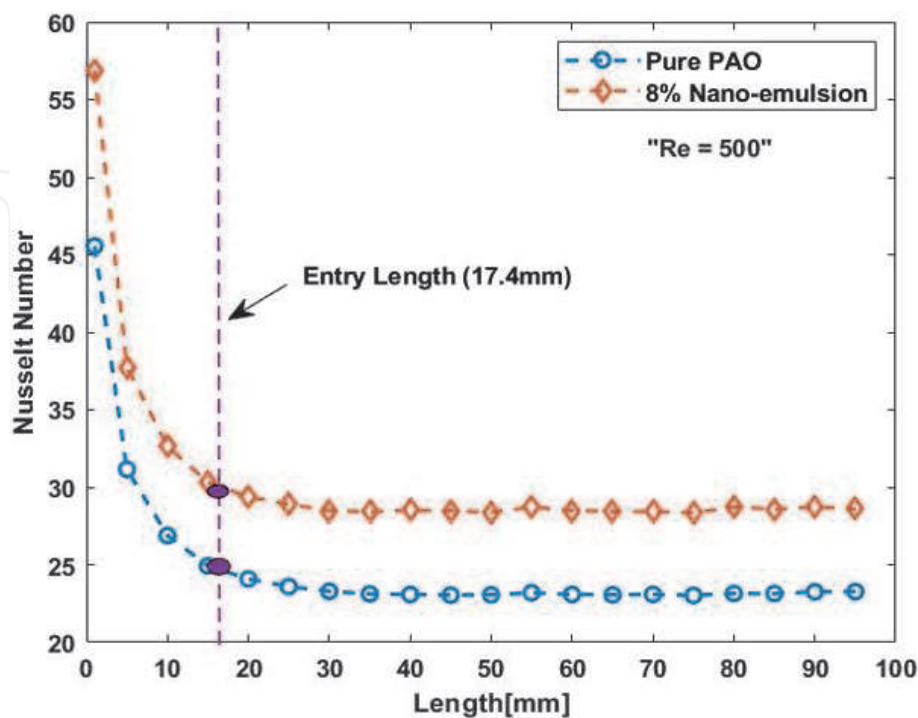

Figure 19.
Friction factor versus Reynolds number for the pure PAO fluid in both minichannel and microchannel heat exchangers.

numbers. Similar to the heat transfer measurements, the friction factor measurements were compared and validated with classical empirical correlations proposed in the literature. As illustrated in **Figure 19**, the friction factor of the PAO fluid flowing inside the minichannel agrees well with the classical Hagen-Poiseuille correlation within the laminar regime. Considering the relatively large dimensions of the microchannel ($H = 780\mu m \times W = 640\mu m$), Baharmi model [89] underestimates the frication factor, and it is likely due to the rough internal surface of the DMLS manufactured microchannel as discussed earlier.

4.2.2 Simulation results

The prototype of the microchannel heat exchanger was designed using CREO software and then the model was imported to COMSOL-Multiphysics to conduct numerical heat transfer analysis for the same geometry and operating conditions summarized in **Table 5**. The following assumptions were adopted to conduct the simulations: no slip boundary condition, normal inflow velocity, uniform wall heat flux boundary conditions imposed on the top and bottom surfaces of the microchannel heat exchanger, and thermophysical properties of the working fluids are set to remain constant for the values listed earlier in **Table 4**. To confirm mesh independency of the simulation results and compare their accuracies, three types of meshes were developed, including finer, fine, and normal. The finer mesh size was ultimately chosen as it provides sufficiently accurate analysis while still sustaining a reasonable computational time.

Figure 20 represents the variations of local Nusselt number at a certain Reynolds number of 500 along the microchannel heat exchanger with the same geometry and dimensions used previously for the experimental investigations as listed in **Table 5**. As shown in this figure, the local Nusselt number decreases along the microchannel at early positions and then reaches relatively constant values of 22 and 29 for the pure PAO and 8 wt% Ethanol/PAO nanoemulsion, respectively, within the fully developed laminar region. This reveals a heat transfer enhancement of around 32%

Figure 20.
Variations of local Nusselt number along the microchannel at Re = 500 for pure PAO and 8% ethanol/PAO nanoemulsion fluids with the entrance effects.

at a certain Reynolds number of 500 using the 8 wt% nanoemulsion fluid compared to that of the pure PAO inside the microchannel heat exchanger.

This is important to note that while the simulation results in **Figure 20** show a Nusselt value of 22 for the fully developed flow of pure PAO, the experimental results introduced in **Figure 18** show a Nusselt value of almost 20 at the same Reynolds of 500, which indicates a relative deviation of approximately 10% between the simulation and experimental results. This deviation is mainly due to the development of model which fails to study the effect of the DMLS manufactured surfaces on the flow and heat transfer characteristics.

As vividly seen from the simulation results in **Figure 20**, there is a declining trend of local Nusselt number along the early locations of the microchannel. The significantly higher Nusselt number at the early locations and its subsequent sharp drop is due to the thermal entrance region at the inlet of the microchannel test section where the internal liquid single-phase flows are still neither thermally nor hydrodynamically fully developed. As a result of having a thermally developing flow in the entrance region, the thermal boundary layer is extremely thin which causes larger values of Nusselt and HTC compared to those of locations outside the entrance region where both of the working fluids are fully developed.

Using the Eq. (13), the hydrodynamic entry length for the laminar flows of PAO and nanoemulsion in the microchannel was found to be 17.5 mm. As illustrated in **Figure 20**, the local Nusselt numbers for each of the working fluids take relatively constant values after the entry length of 17.5 mm where the boundary layer develops fully across the cross section of the microchannel and appears to be independent of the channel length. Since the working fluids are PAO and nanoemulsion with Prandtl numbers greater than 1 ($Pr > 1$), the hydrodynamic boundary layer develops more quickly than the thermal boundary layer.

5. Conclusions

In this study, the flow and heat transfer characteristics of a novel nanostructured heat transfer fluid (i.e., ethanol/polyalphaolefin nanoemulsion) inside a minichannel of circular cross section and a microchannel of rectangular cross sec-tion were investigated experimentally and numerically. The experiments were performed for single-phase flow of pure PAO and ethanol/PAO nanoemulsion fluids of 4 wt% and 8 wt% concentrations within the laminar and transitional regimes as well as for two-phase flow boiling of nanoemulsion fluids within the laminar flow regime.

It was revealed that the nanoemulsion fluids thermally outperformed the pure PAO base fluid in single-phase flow of transitional regime, however, it does not reflect an appreciable improvement in single-phase heat transfer performance within the laminar flow regime. The significant heat transfer enhancement achieved at higher concentrations of nanoemulsion within the transitional regime is mainly attributed to the enhanced interaction and interfacial thermal transport between ethanol nanodroplets and PAO base fluid. For two-phase flow boiling, heat transfer coefficients of ethanol/PAO nanoemulsion fluids were further enhanced once the ethanol nanodroplets underwent phase change. A comparative study was also conducted on the flow and heat transfer characteristics of pure PAO between the traditionally manufactured minichannel and additively manufactured microchannel under the same operating conditions. Despite the higher friction factor and pressure loss, significant heat transfer enhancements were achieved using the additively manufactured microchannel compared to the traditionally fab-ricated minichannel heat exchanger under the same operating conditions, so that

the gained heat transfer enhancement through the microchannel is more prominent than its drawback of increased pressure loss. The non-post processed surface of the DMLS manufactured microchannel is believed to be the main contributor to the augmented heat transfer and pressure drop. Further studies are needed to fully understand the possible mechanisms behind it, and also to gain a deeper insight into the phase-change heat transfer characteristics of nanoemulsion fluids.

Acknowledgements

Author details

Jaime Rios, Mehdi Kabirnajafi, Takele Gameda, Raid Mohammed and Jiajun Xu*
Center for Advanced Manufacturing in Space Technology and Applied Research (CAM-STAR), University of the District of Columbia, Washington D.C., USA

*Address all correspondence to: jiajun.xu@udc.edu

IntechOpen

References

[1] Kabirnajafi, M., Xu, J. Experimental Approaches to Measurement of Vapor Quality of Two-Phase Flow Boiling. Heat Transfer - Design, Experimentation and Applications, INTECH, Edited by Miguel Araiz, 2020, ISBN: 978-1-83968-438-8.

[2] Kandlikar, S.G., Steinke, M.E. Examples of microchannel mass transfer processes in biological systems, Proceedings of 1st International Conference on Minichannels and Microchannels, Rochester, NY, April 24–25, 2003, Paper ICMM2003–1124, ASME 933–943.

[3] Kandlikar, S.G., Garimella, S., Li, D., Colin, S., King, M. Heat transfer and fluid flow in minichannels and microchannels, Elsevier, 2006, ISBN: 0-0804-4527-6.

[4] Mehendale, S.S., Jacobi, A.M., Shah, R.K. Fluid flow and heat transfer at micro- and meso-scales with applications to heat exchanger design. Appl. Mech. Rev., 2000, 53: 175–193.

[5] Kandlikar, S.G., Grande, W.J. Evolution of microchannel flow passages – thermohydraulic performance and fabrication technology, Heat Transfer Eng., 2003, 24: 3–17.

[6] Cheng, P., Wu, H.Y., Hong, F.J. Phase-change heat transfer in microsystems, J. Heat Transfer, Trans. ASME, 2007, 129: 101–107.

[7] Dewan, A., Mahanta, P., Raju, K. S., and Kumar, P. S., 2004, "Review of passive heat transfer augmentation techniques," Proceedings of the Institution of Mechanical Engineers Part a-Journal of Power and Energy, 218 (A7), pp. 509–527.t

[8] Agostini, B., Fabbri, M., Park, J. E., Wojtan, L., Thome, J. R., and Michel, B., 2007, "State of the art of high heat flux

cooling technologies," Heat Transfer Engineering, 28(4), pp. 258–281.

[9] Ebadian, M. A., and Lin, C. X., 2011, "A Review of High-Heat-Flux Heat Removal Technologies," Journal of Heat Transfer-Transactions of the Asme, 133 (11).

[10] Inaba, H., 2000, "New challenge in advanced thermal energy transportation using functionally thermal fluids," International Journal of Thermal Sciences, 39(9–11), pp. 991–1003.

[11] Zimparov, V., 2002, "Energy conservation through heat transfer enhancement techniques," International Journal of Energy Research, 26(7), pp. 675–696.

[12] Xuan, Y. M., and Li, Q., 2003, "Investigation on convective heat transfer and flow features of nanofluids," Journal of Heat Transfer-Transactions of the Asme, 125(1), pp. 151–155.

[13] Evans, W., Fish, J., and Keblinski, P., 2006, "Role of Brownian motion hydrodynamics on nanofluid thermal conductivity," Applied Physics Letters, 88(9).

[14] Heris, S. Z., Etemad, S. G., and Esfahany, A. N., 2006, "Experimental investigation of oxide nanofluids laminar flow convective heat transfer," International Communications in Heat and Mass Transfer, 33(4), pp. 529–535.

[15] Kim, S. J., Bang, I. C., Buongiorno, J., and Hu, L. W., 2006, "Effects of nanoparticle deposition on surface wettability influencing boiling heat transfer in nanofluids," Applied Physics Letters, 89(15).

[16] Ma, H. B., Wilson, C., Borgmeyer, B., Park, K., Yu, Q., Choi, S. U. S., and Tirumala, M., 2006, "Effect of

nanofluid on the heat transport capability in an oscillating heat pipe," Applied Physics Letters, 88(14).

[17] Prasher, R., Song, D., Wang, J. L., and Phelan, P., 2006, "Measurements of nanofluid viscosity and its implications for thermal applications," Applied Physics Letters, 89(13).

[18] Chein, R., and Chuang, J., 2007, "Experimental microchannel heat sink performance studies using nanofluids," International Journal of Thermal Sciences, 46(1), pp. 57–66.

[19] Khodadadi, J. M., and Hosseinizadeh, S. F., 2007, "Nanoparticle-enhanced phase change materials (NEPCM) with great potential for improved thermal energy storage," International Communications in Heat and Mass Transfer, 34(5), pp. 534–543.

[20] Buongiorno, J., Hu, L. W., Kim, S. J., Hannink, R., Truong, B., and Forrest, E., 2008, "Nanofluids for enhanced economics and safety of nuclear reactors: An evaluation of the potential features, issues, and research gaps," Nuclear Technology, 162(1), pp. 80–91.

[21] Coursey, J. S., and Kim, J., 2008, "Nanofluid boiling: The effect of surface wettability," International Journal of Heat and Fluid Flow, 29(6), pp. 1577–1585.

[22] Milanova, D., and Kumar, R., 2008, "Heat transfer behavior of silica nanoparticles experiment in pool boiling," Journal of Heat Transfer-Transactions of the Asme, 130(4).

[23] Merabia, S., Keblinski, P., Joly, L., Lewis, L. J., and Barrat, J. L., 2009, "Critical heat flux around strongly heated nanoparticles," Physical Review E, 79(2), p. 4.

[24] Shima, P. D., Philip, J., and Raj, B., 2009, "Magnetically controllable nanofluid with tunable thermal conductivity and viscosity," Applied Physics Letters, 95(13).

[25] Wang, L. Q., and Wei, X. H., 2009, "Nanofluids: Synthesis, Heat Conduction, and Extension," Journal of Heat Transfer-Transactions of the Asme, 131(3).

[26] Boudouh, M., Gualous, H. L., and De Labachelerie, M., 2010, "Local convective boiling heat transfer and pressure drop of nanofluid in narrow rectangular channels," Applied Thermal Engineering, 30(17–18), pp. 2619–2631.

[27] Wong, K. V., and De Leon, O., 2010, "Applications of Nanofluids: Current and Future," Advances in Mechanical Engineering, p. 11.

[28] Yu, W., Xie, H. Q., Wang, X. P., and Wang, X. W., 2011, "Significant thermal conductivity enhancement for nanofluids containing graphene nanosheets," Physics Letters A, 375(10), pp. 1323–1328.

[29] Hampton, M. A., Nguyen, T. A. H., Nguyen, A. V., Xu, Z. P., Huang, L. B., and Rudolph, V., 2012, "Influence of surface orientation on the organization of nanoparticles in drying nanofluid droplets," Journal of Colloid and Interface Science, 377, pp. 456–462.

[30] Park, S. D., Lee, S. W., Kang, S., Kim, S. M., and Bang, I. C., 2012, "Pool boiling CHF enhancement by graphene-oxide nanofluid under nuclear coolant chemical environments," Nuclear Engineering and Design, 252, pp. 184–191.

[31] Chehade, A. A., Gualous, H. L., Le Masson, S., Fardoun, F., and Besq, A., 2013, "Boiling local heat transfer enhancement in minichannels using nanofluids," Nanoscale Research Letters, 8, pp. 1–20.

[32] Hadad, K., Rahimian, A., and Nematollahi, M. R., 2013, "Numerical

study of single and two-phase models of water/Al2O3 nanofluid turbulent forced convection flow in VVER-1000 nuclear reactor," Annals of Nuclear Energy, 60, pp. 287–294.

[33] Ray, D. R., Das, D. K., and Vajjha, R. S., 2014, "Experimental and numerical investigations of nanofluids performance in a compact minichannel plate heat exchanger," International Journal of Heat and Mass Transfer, 71, pp. 732–746.

[34] Yu, L. Y., Sur, A., and Liu, D., 2015, "Flow Boiling Heat Transfer and Two-Phase Flow Instability of Nanofluids in a Minichannel," Journal of Heat Transfer-Transactions of the Asme, 137(5).

[35] Roesle, M. L., and Kulacki, F. A., 2010, "Boiling of Dilute Emulsions-Toward a New Modeling Framework," Industrial & Engineering Chemistry Research, 49(11), pp. 5188–5196.

[36] Morshed, A., Paul, T. C., Fang, R. X., Khan, J. A., and Asme, 2013, "Flow boiling Characteristics of Dilute Emulsion in Microchannel," Proceedings of the Asme International Mechanical Engineering Congress and Exposition - 2012, Vol 7, Pts a-D, pp. 2085-2091.

[37] Kotlarchyk, M., Chen, S. H., and Huang, J. S., 1982, "TEMPERATURE-DEPENDENCE OF SIZE AND POLYDISPERSITY IN A 3-COMPONENT MICRO-EMULSION BY SMALL-ANGLE NEUTRON-SCATTERING," Journal of Physical Chemistry, 86(17), pp. 3273–3276.

[38] Bulanov, N. V., Skripov, V. P., and Khmylnin, V. A., 1984, "Heat Transfer to Emulsion with superheating of its disperse phase," J. Eng. Phys., pp. 1-3.

[39] Bulanov, N. V., Skripov, V. P., and Khmylnin, V. A., 1993, "Heat Transfer to Emulsion with a low-boiling disperse phase," Heat Transfer Res, pp. 786-789.

[40] Bulanov, N. V., 2001, "An analysis of the heat flux density under conditions of boiling internal phase of emulsion," High Temperature, 39(3), pp. 462–469.

[41] Bulanov, N. V., Gasanov, B. M., and Turchaninova, E. A., 2006, "Results of experimental investigation of heat transfer with emulsions with low-boiling disperse phase," High Temperature, 44(2), pp. 267–282.

[42] Choi, S. U. S., and Eastman, J. A., 1995, ASME International Mechanical Engineering Congress & Expositio.

[43] Moore, G. R., 1959, "Vaporization of Superheated Drops in Liquids," Aiche Journal, 5(4), pp. 458–466.

[44] Bulanov, N. V., and Gasanov, B. M., 2005, "Experimental setup for studying the chain activation of low-temperature boiling sites in superheated liquid droplets," Colloid Journal, 67(5), pp. 531–536.

[45] Bulanov, N. V., and Gasanov, B. M., 2008, "Peculiarities of boiling of emulsions with a low-boiling disperse phase," International Journal of Heat and Mass Transfer, 51(7–8), pp. 1628–1632.

[46] Rosele, M. L., 2010, "Boiling of Dilute Emulsions," PhD dissertation, University of Minnesota.

[47] Trinh V., Xu J., An Experimental Study on Flow and Heat Transfer Characteristics of Ethanol/Polyalphaolefin Nanoemulsion Flowing Through Circular Minichannels. Nanoscale Research Letters, 2017, 12: 216. DOI 10.1186/s11671-017-1984-1.

[48] Kumar, P., and Mittal, K. L., 1999, Handbook of microemulsion science and technology, New York: Marcel Dekker.

[49] Shanthi, R., Anandan, S. S., and Ramalingam, V., 2012, "HEAT

TRANSFER ENHANCEMENT USING NANOFLUIDS: An Overview," Thermal Science, 16(2), pp. 423–444.

[50] Wang, X. Q., and Mujumdar, A. S., 2008, "A REVIEW ON NANOFLUIDS - PART I: THEORETICAL AND NUMERICAL INVESTIGATIONS," Brazilian Journal of Chemical Engineering, 25(4), pp. 613–630.

[51] Kakac, S., and Pramuanjaroenkij, A., 2009, "Review of convective heat transfer enhancement with nanofluids," International Journal of Heat and Mass Transfer, 52(13–14), pp. 3187–3196.

[52] Murshed, S.M., Nieto de Castro, C. A., Lourenco, M. J. V., Lopes, M. L. M., and Santos, F. J. V., 2011, "A review of boiling and convective heat transfer with nanofluids," Renewable & Sustainable Energy Reviews, 15(5), pp. 2342–2354.

[53] Wang, X. Q., and Mujumdar, A. S., 2008, "A REVIEW ON NANOFLUIDS - PART II: EXPERIMENTS AND APPLICATIONS," Brazilian Journal of Chemical Engineering, 25(4), pp. 631–648.

[54] Yang, B., and Han, Z. H., 2006, "Thermal conductivity enhancement in water-in-FC72 nanoemulsion fluids," Applied Physics Letters, 88(26).

[55] Han, Z. H., and Yang, B., 2008, "Thermophysical characteristics of water-in-FC72 nanoemulsion fluids," Applied Physics Letters, 92(1).

[56] Xu, J., Liu, X., Yang, B., 2009, THERMOPHYSICAL CHARACTERISTICS OF SELF-ASSEMBLED ETHANOL/ POLYALPHAOLEFIN NANOEMULSION FLUIDS. ASME IMECE 2009, Nov. 13-19, 2023–2026.

[57] Xu, J., Wu, C. W., and Yang, B., 2010, "Thermal- and Phase-Change Characteristics of Self-Assembled Ethanol/Polyalphaolefin Nanoemulsion Fluids," Journal of Thermophysics and Heat Transfer, 24(1), pp. 208–211.

[58] Han, Z. H., Yang, B., Qi, Y., and Cumings, J., 2011, "Synthesis of low-melting-point metallic nanoparticles with an ultrasonic nanoemulsion method," Ultrasonics, 51(4), pp. 485–488.

[59] Xu, J., Yang, B., and Hammouda, B., 2011, "Thermal conductivity and viscosity of self-assembled alcohol/ polyalphaolefin nanoemulsion fluids," Nanoscale Research Letters, 6.

[60] Xu, J., Hammouda, B., and Yang, B., 2012, "Thermophysical Properties and Pool Boiling Characteristics of Water in Polyalphaolefin Nanoemulsion Fluids," ASME, Proceedings of ASME Micro/ Nanoscale Heat & Mass Transfer International Conference 2012.

[61] Xu, J., and Yang, B., 2012, "Novel Heat Transfer Fluids: Self-assembled Nanoemulsion Fluids," Nanotechnology, D.J.N. Govil, ed., Studium Press LLC.

[62] Xu, J., Yang, B., and Hammouda, B., 2013, "Thermophysical Properties and Pool Boiling Characteristics of Water-in-Polyalphaolefin Nanoemulsion Fluids," Journal of Heat Transfer-Transactions of the Asme, 135(9).

[63] Xu, J., Hammouda, B., Cao, F., and Yang, B., 2015, "Experimental study of thermophysical properties and nanostructure of self-assembled water/ polyalphaolefin nanoemulsion fluids," Advances in Mechanical Engineering, 7 (4): 1–8.

[64] Xu, J., Yang, B., 2012, Thermophysical Properties and Pool Boiling Characteristics of Water in Polyalphaolefin Nanoemulsion Fluids. ASME 2012, Int. Conference on Micro/ Nanoscale Heat and Mass Transfer, Atlanta, GA, USA. MNHMT2012-75232, 321-325.

[65] Kandlikar, S.G., Grande, W.J. Evaluation of single-phase flow in microchannels for high heat flux chip cooling—thermohydraulic performance enhancement and fabrication technology. Heat Transfer Eng., 2004, 25(8): 5–16.

[66] Cooke, D., Kandlikar, S.G. Pool boiling heat transfer and bubble dynamics over plain and enhanced microchannels. J Heat Transfer Trans ASME, 2011, 133(5):052902–052901.

[67] Ahn, H.S., Sathyamurthi, V., and Banerjee, D., 2009, "Pool Boiling Experiments on a Nano-Structured Surface," IEEE Transactions on Components and Packaging Technologies, 32(1), pp. 156–165.

[68] Sathyamurthi, V., Ahn, H. S., Banerjee, D., and Lau, S. C., 2009, "Subcooled Pool Boiling Experiments on Horizontal Heaters Coated with Carbon Nanotubes," Journal of Heat Transfer-Transactions of the ASME, 131(7).

[69] Morshed, A., Rezwana, A. A., and Khan, J. A., 2014, "Two-phase convective flow in microchannel with nanoporous coating," 10th International Conference on Mechanical Engineering (ICME 2013), 90, pp. 588-598.

[70] Kumar, C. S. S., Suresh, S., Aneesh, C. R., Kumar, M. C. S., Praveen, A. S., and Raji, K., 2015, "Flow boiling heat transfer enhancement on copper surface using Fe doped Al2O3-TiO2 composite coatings," Applied Surface Science, 334, pp. 102–109.

[71] Hammouda, B., SANS from Polymers-Review of the Recent Literature. Polymer Reviews 2010, 50 (1), 14–39.

[72] Hammouda, B.; Krueger, S.; Glinka, C. J., Small-angle neutron scattering at the national institute of standards and technology. Journal of Research of the National Institute of Standards and Technology 1993, 98 (1), 31–46.

[73] Bergman T.A., Levine A.S., Incropera F.P., Dewitt D.P., Fundamentals of Heat and Mass Transfer, John Wiley & Sons Inc., 7th Edition, 2011, ISBN 13 978–0470–50197-9.

[74] Abraham JP, Sparrow EM, Minkowycz WJ., 2011, Internal-flow Nusselt numbers for the low-Reynolds-number end of the laminar-to-turbulent transition regime. Int J Heat Mass Transf 54:584–588.

[75] Frazier, W. E., 2014, "Metal Additive Manufacturing: A Review," Journal of Materials Engineering and Performance, 23(6), pp. 1917–1928.

[76] Mellor, S., Hao, L., and Zhang, D., 2014, "Additive manufacturing: A framework for implementation," International Journal of Production Economics, 149, pp. 194–201.

[77] Yap, C. Y., Chua, C. K., Dong, Z. L., Liu, Z. H., and Zhang, D. Q., 2014, STATE-OF-THE-ART REVIEW ON SELECTIVE LASER MELTING OF NON-FERROUS METALS.

[78] Giannatsis, J., and Dedoussis, V., 2009, "Additive fabrication technologies applied to medicine and health care: a review," International Journal of Advanced Manufacturing Technology, 40(1–2), pp. 116–127.

[79] Levy, G. N., Schindel, R., and Kruth, J. P., 2003, "Rapid manufacturing and rapid tooling with layer manufacturing (LM) technologies, state of the art and future perspectives," Cirp Annals-Manufacturing Technology, 52(2), pp. 589–609.

[80] Longhitano, G. A., Larosa, M. A., Munhoz, A. L. J., Zavaglia, C. A. D., and Ierardi, M. C. F., 2015, "Surface Finishes for Ti-6Al-4V Alloy Produced by Direct

Metal Laser Sintering," Materials Research-Ibero-American Journal of Materials, 18(4), pp. 838–842.

[81] Kruth, J. P., Wang, X., Laoui, T., and Froyen, L., 2003, "Lasers and materials in selective laser sintering," Assembly Automation, 23(4), pp. 357–371.

[82] Gibson, I., and Shi, D. P., 1997, "Material properties and fabrication parameters in selective laser sintering process," Rapid Prototyping Journal, 3 (4), pp. 129–136.

[83] Krauss, H., Zeugner, T., and Zaeh, M. F., 2015, "Thermographic Process Monitoring in Powderbed Based Additive Manufacturing," Proc. 41st Annual Review of Progress in Quantitative Nondestructive Evaluation (QNDE), pp. 177-183.

[84] Stimpson, C. K., Snyder, J. C., Thole, K. A., and Mongillo, D., 2016, "Roughness Effects on Flow and Heat Transfer for Additively Manufactured Channels," Journal of Turbomachinery, 138(5), pp. 051008-051008-051010.

[85] Snyder, J. C., Stimpson, C. K., Thole, K. A., and Mongillo, D., 2016, "Build Direction Effects on Additively Manufactured Channels," Journal of Turbomachinery, 138(5), pp. 051006-051006-051008.

[86] Sadaghiani, A. K., Saadi, N. S., Parapari, S. S., Karabacak, T., Keskinoz, M., and Kosar, A., 2017, "Boiling heat transfer performance enhancement using micro and nano structured surfaces for high heat flux electronics cooling systems," Applied Thermal Engineering, 127, pp. 484–498.

[87] Zhang, J., Diao, Y. H., Zhao, Y. H., and Zhang, Y. N., 2017, "An experimental investigation of heat transfer enhancement in minichannel: Combination of nanofluid and micro fin structure techniques," Experimental Thermal and Fluid Science, 81, pp. 21–32.

[88] Harirchian, T., and Garimella, S. V., 2008, "Microchannel size effects on local flow boiling heat transfer to a dielectric fluid," International Journal of Heat and Mass Transfer, 51(15–16), pp. 3724–3735.

[89] Bahrami, M., Yovanovich, M. M., and Culham, J. R., 2006, "Pressure Drop of Fully-Developed, Laminar Flow in Microchannels of Arbitrary Cross-Section," Journal of Fluids Engineering, 128(5):1036–1044.